ACADEMIC PRESS

Available online at www.sciencedirect.com
SCIENCE DIRECT®

Journal of Catalysis 217 (2003) 222–232

JOURNAL OF CATALYSIS

www.elsevier.com/locate/jcat

Structure and support effects on the selective oxidation of dimethyl ether to formaldehyde catalyzed by MoO_x domains

Haichao Liu, Patricia Cheung, and Enrique Iglesia *

Department of Chemical Engineering, University of California at Berkeley, Berkeley, CA 94720, USA

Received 4 November 2002; revised 13 January 2003; accepted 13 January 2003

Abstract

The selective oxidation of dimethyl ether (CH_3OCH_3) to formaldehyde (HCHO) was carried out on MoO_x species with a wide range of MoO_x surface density and structure supported on MgO, Al_2O_3, ZrO_2, and SnO_2. Raman and X-ray absorption spectroscopies were used to probe the structure of these MoO_x domains, as they evolved from monomeric species into two-dimensional polymolybdate domains and MoO_3 clusters with increasing MoO_x surface density. Primary HCHO synthesis rates (per Mo atom) initially increased with increasing MoO_x surface density (1.5–7 Mo/nm^2) on all supports, indicating that MoO_x domain surfaces become more active as two-dimensional monolayers form via oligomerization of monomer species. The incipient formation of MoO_3 clusters at higher surface densities led to inaccessible MoO_x species and to lower HCHO synthesis rates (per Mo). Areal rates reached constant values as polymolybdate monolayers formed. These areal rates depend on the identity of the support; they were highest on SnO_2, lowest on Al_2O_3, and undetectable on MgO, indicating that the surface properties of polymolybdate structures are strongly influenced by their atomic attachment to a specific support. The catalytic behavior of MoO_x domains reflects their ability to delocalize electron density during the formation of transition states required for rate-determining C–H bond activation steps within redox cycles involved in HCHO synthesis from dimethyl ether. These conclusions are consistent with the observed parallel increase in the rates of HCHO synthesis and of incipient stoichiometric reduction of MoO_x domains by H_2 as the domain size increases and as the supports become less insulating and more reducible, and as the energy required for ligand-to-metal electronic transitions in the UV–visible spectrum decreases. HCHO selectivities increased with increasing MoO_x domain size; they were highest on Al_2O_3 and lowest on SnO_2 supports. The Lewis acidity of the support cations appears to influence HCHO binding energy. HCHO reactions leading to CO_x and methyl formate via primary and secondary pathways are favored on weaker Lewis acids (with stronger conjugate bases). The Mo–O–support linkages prevalent at low surface densities also favor primary and secondary pathways to CO_x and methyl formate. When reported on a CH_3OH-free basis, because of the pathways available for CH_3OH oxidation to HCHO and for CH_3OCH_3–CH_3OH interconversion, primary HCHO selectivities reached values greater than 95% on Al_2O_3-supported polymolybdate monolayers.

Keywords: Dimethyl ether oxidation; Formaldehyde synthesis; Molybdenum oxide catalysts; Support effects

1. Introduction

The significant thermodynamic and kinetic hurdles for the direct conversion of CH_4 to alkenes and oxygenates have led to alternate processes involving synthesis gas intermediates [1–5]. For example, oxidative dehydrogenation of methanol is used to manufacture formaldehyde (HCHO) [6,7], which is then used as an intermediate to produce larger molecules containing C–C bonds. Recent advances in the synthesis of dimethyl ether (DME; CH_3OCH_3) from H_2/CO mixtures [8–10] and the anticipated similarities in the catalytic chemistries of DME and methanol on oxide surfaces [11,12] led us to consider DME as a cheaper and less toxic intermediate for the synthesis of chemicals currently produced from methanol. Previous studies reported low rates and selectivities for the catalytic conversion of DME to HCHO [13–18]. Recently, we have shown that MoO_x and VO_x domains supported on Al_2O_3, ZrO_2, and SnO_2 catalyze this reaction with high primary HCHO selectivities (80–98% HCHO, CH_3OH-free basis) and high reaction rates at temperatures much lower than in previous studies (500–550 K vs 773 K) [19].

* Corresponding author.
E-mail address: iglesia@cchem.berkeley.edu (E. Iglesia).

0021-9517/03/$ – see front matter
doi:10.1016/S0021-9517(03)00025-3

We have also previously reported the effects of the size and structure of ZrO_2-supported MoO_x domains on primary and secondary DME reaction rates [20]. Here, we report the significant effects of oxide supports on the structure, reducibility, and catalytic properties of active MoO_x domains. The acid–base properties [21,22], the surface charge [23,24], and the electronegativity of support cations [25,26] are often implicated in many support effects, but clear evidence of their specific involvement remains elusive. We present here a detailed study of selective DME oxidation reactions on MoO_x domains supported on MgO, Al_2O_3, ZrO_2, and SnO_2 with a wide range of Mo surface density. We also examine the structure of these materials using complementary X-ray diffraction and Raman and X-ray absorption spectroscopic methods. These supports show a wide range of acid–base and redox surface properties. MgO and Al_2O_3 are unreducible oxides with basic and acid surfaces, respectively. ZrO_2 and SnO_2 are amphoteric oxides with surface sites that can undergo redox cycles and catalyze dehydrogenation steps. These support materials are used here to probe support effects on the structure and redox and catalytic properties of dispersed MoO_x domains, with specific emphasis on the rational design of selective catalysts for the conversion of dimethyl ether to formaldehyde.

2. Experimental

2.1. Synthesis of catalytic materials

Supported MoO_x catalysts were prepared by incipient wetness impregnation of $ZrO(OH)_2$, SnO_2, or MgO with aqueous $(NH_4)_2Mo_2O_8$ (99%, Aldrich) solutions. $ZrO(OH)_2$ was prepared by hydrolysis of aqueous zirconyl chloride solutions (> 98%, Aldrich) at a pH of ∼ 10 using NH_4OH (14.8 N, Fisher Scientific), followed by filtration of the precipitated powders and drying at 393 K overnight [27]. SnO_2 was prepared by hydrolysis of tin(IV) chloride pentahydrate (98%, Alfa Aesar) at a pH of ∼ 7 using NH_4OH (14.8 N, Fisher Scientific). The precipitates were washed with deionized water until a Ag nitrate test failed to detected Cl ions in the effluent. The resulting solids were treated in flowing dry air (Airgas, zero grade) at 773 K for 3 h. MgO supports were prepared by treating MgO (> 98%, Aldrich) with deionized water at 355–365 K for 4 h, and then treating samples in flowing dry air (Airgas, zero grade) at 773 K for 8 h. Al_2O_3-supported MoO_x catalysts were also prepared by incipient wetness impregnation, using γ-Al_2O_3 (Degussa, AG) and an aqueous $(NH_4)_6Mo_7O_{24}$ (99%, Aldrich) solution at pH 5 [28]. The Mo content was varied by changing the Mo concentration in the impregnating solutions. All samples were dried at 393 K in ambient air after impregnation and then treated in flowing dry air (Airgas, zero grade) at 773 K for 3 h. Bulk MoO_3 was prepared by decomposition of $(NH_4)_2Mo_2O_8$ (99%, Aldrich) in dry air at 773 K for 3 h. The Mo surface density for all supported samples is reported as Mo/nm^2 per square nanometers based on the Mo content and the BET surface area for each sample.

2.2. Structural characterization

Surface areas were measured using N_2 at its normal boiling point (Autosorb-1; Quantachrome) and BET analysis methods. Powder X-ray diffraction patterns were measured at ambient conditions using a Siemens D-5000 diffractometer, Cu-K_α radiation ($\lambda = 1.5418$ Å), and a scan rate of 0.07° s^{-1}.

Raman spectra were measured using a HoloLab 5000 Raman spectrometer (Kaiser Optical) and a frequency-doubled Nd:YAG laser at a wavelength of 532 nm. Samples were pressed into self-supporting thin wafers, placed on a rotary stage within a quartz cell, and spun at ∼ 16 Hz to avoid structural changes caused by laser local heating. The spectra were collected by exposure of the samples to laser for 6 s at a laser power of 50 mW and averaging of 100 spectra. Raman spectra were measured at 298 K for fresh and dehydrated samples. Dehydration was carried out in situ at 773 K for 1 h in flowing 20% O_2/He.

Mo K-edge X-ray absorption spectra were measured using beamline 4-1 at the Stanford Synchrotron Radiation Laboratory. Samples were diluted with Al_2O_3 for MoO_x/Al_2O_3 samples or with SiO_2 for all other samples to achieve a Mo content of ∼ 5 wt% and then pelletized and sieved to retain particles 0.18–0.25 mm in diameter. The particles were placed within a thin quartz capillary tube (1.0-mm od, 0.1-mm thickness) supported horizontally within a heated compartment held in the path of the rectangular X-ray beam (0.2×6.0 mm) [29]. X-ray absorption spectra were measured in transmission mode with Ar gas in three ion chamber detectors: one chamber was located before the sample to measure the incident X-ray intensity, another chamber was located after the sample and before a Mo reference foil, and the third chamber was placed after the Mo foil. The incident beam energy was selected using a Si (111) crystal monochromator with 5-eV increments in the pre-edge region (19.875–19.975 keV), 0.25-eV increments in the edge region (19.975–20.035 keV), and 0.04 Å^{-1} in the fine structure region (20.035–21.024 keV). Energies were calibrated by placing the first inflection point in the Mo foil spectrum at its known absorption energy (19.999 keV). The spectra were analyzed using WinXAS (Version 1.2) [30]. A linear fit to the pre-edge region was subtracted from the entire spectrum, and then the spectrum was normalized with a third order polynomial. After conversion to k-space, the k^3-weighed fine structure spectrum was Fourier-transformed between 2.0 and 16.0 Å.

2.3. Reducibility of supported MoO_x samples in H_2

Reduction rates for MoO_x/ZrO_2 samples with Mo surface densities of 0.5–6.4 Mo/nm^2 and for MoO_x/Al_2O_3 (7.0

Mo/nm^2) and MoO_x/MgO (5.8 Mo/nm^2) in H_2 were measured using a surface area analyzer (Quantachrome) modified with electronic mass flow controllers. The sample temperature was increased from 298 to 1253 K at 0.167 K s^{-1} in flowing 20% H_2/Ar (1.33 cm^3 s^{-1}; Matheson UHP, certified mixture). An amount of sample containing 10 mg Mo was placed within a quartz cell. The H_2 concentration in the effluent stream was measured using a thermal conductivity detector after the water formed during reduction was removed using a 13X molecular sieve held at ambient temperature. The thermal conductivity response was calibrated from the reduction of pure CuO powder (99.995%, Aldrich). Initial oxygen removal rates were calculated from these data using kinetic analysis methods previously reported [28,31].

MoO_x reduction rates in H_2 were also measured for MoO_x/SnO_2 (6.3 Mo/nm^2), MoO_x/ZrO_2 (6.4 Mo/nm^2), and MoO_x/Al_2O_3 (7.0 Mo/nm^2) using in situ X-ray absorption spectroscopy (XANES) (Mo *K*-edge). Near-edge absorption spectra were measured using a Si (111) crystal monochromator with 5-eV increments in the pre-edge region (19.905–19.990 keV), 0.50-eV increments in the edge region (19.990–20.033 keV), and 0.04 Å^{-1} in the fine structure region (20.033–20.700 keV). In this approach, the extent of reduction of Mo^{6+} to Mo^{4+} was subtracted from the XANES spectra analyzed between 19.990 and 20.120 keV using linear superimposition methods [28] and the spectra of bulk MoO_2 and of Mo^{6+} in the fresh catalyst samples.

2.4. Catalytic dimethyl ether reactions

Dimethyl ether reactions were carried out at 453–553 K in a fixed-bed quartz microreactor using supported MoO_x samples (0.15–0.30 g) diluted with acid-washed quartz powder (∼ 1 g) to prevent temperature gradients. Samples were treated in flowing 20% O_2/He (0.67 cm^3 s^{-1}) for 1.5 h at 773 K before catalytic measurements. The reactant mixture consisted of 80 kPa DME (99.5%, Praxair), 18 kPa O_2, and 2 kPa N_2 (2 kPa) (Praxair, certified O_2/N_2 mixture). Homogeneous dimethyl ether reactions were detected using empty reactors only above 593 K.

The reactor effluent was analyzed by on-line gas chromatography (Hewlett–Packard 6890 GC) using a methyl silicone capillary column (HP-1; 30 m, 0.25 mm, 0.25 μm film) and a Porapak Q packed column (80–100 mesh, 1.82 m, 3.18 mm) connected to flame ionization and thermal conductivity detectors, respectively. Methanol, formaldehyde (HCHO), methyl formate (MF), CO, CO_2, H_2O, and traces of dimethoxymethane (DMM) were the only products detected.

Reaction rates and product selectivities were measured as a function of dimethyl ether conversion, which was varied by changing the reactant space velocity. Reactant conversions were kept below 10%. DME reaction rates and product selectivities were extrapolated to zero residence time to obtain the corresponding primary rates and selectivities. In view of the available pathways for DME–CH_3OH interconversion and for CH_3OH conversion to HCHO, rates and selectivities are reported here, unless noted otherwise, on a methanol-free basis.

3. Results and discussion

3.1. Structural characterization of supported MoO_x catalysts

Fig. 1a shows Raman spectra for fresh MoO_x/SnO_2 samples with a wide range of Mo surface densities (2.1–11.3 Mo/nm^2). Raman bands were detected at 636 (s), 777 (w), 864–870 (s), and 953–967 (s) cm^{-1} on all samples. The bands at 636 and 777 cm^{-1} are assigned to SnO_2 crystallites [24,32,33], while those at 864–870 and 953–967 cm^{-1} correspond to bridging Mo–O–Mo and terminal Mo=O stretching modes in oligomeric MoO_x species, respectively, [24]. At 6.3 Mo/nm^2, an additional shoulder appeared at 825 cm^{-1}, which evolved into a sharp band along with two new bands at 672 and 1001 cm^{-1} as the Mo surface density reached 11.3 Mo/nm^2; these new bands correspond to the incipient formation of crystalline MoO_3 [24] as the surface density increases above that expected for a polymolybdate monolayer (∼ 5 Mo/nm^2) [34].

The band at ∼ 965 cm^{-1} for terminal Mo=O stretches shifted to higher frequencies and split into a doublet (986 and 1003 cm^{-1}) (Fig. 1b) after samples were treated in 20% O_2/He at 773 K; all other bands remained unchanged. The intensity of these two bands (relative to the SnO_2 bands) increased with increasing Mo surface density, in parallel with the observed increase in the intensity of the Mo–O–Mo band at ∼ 865 cm^{-1}. Thus, we conclude that these bands correspond to Mo=O bonds in distorted oligomers (986 cm^{-1}) and monomers (1003 cm^{-1}). Exposure to moisture from ambient air at room temperature led to the coalescence of these two bands into the original feature at ∼ 965 cm^{-1}. This reversible process was first reported by Dumesic and co-workers [32], who used it as evidence for the complete dispersion of MoO_x structures on SnO_2 [32]. The observed shift to higher frequencies on water desorption is associated with a change in Mo coordination and in bond order in terminal Mo=O structures [24].

These results suggest that isolated monomolybdates condense to form oligomeric two-dimensional structures as Mo densities reach ∼ 6 Mo/nm^2 on SnO_2 surfaces and then form crystalline MoO_3 at higher coverages. X-ray diffraction measurements showed lines corresponding to MoO_3 only for surface densities above 6.3 Mo/nm^2. This structural evolution of MoO_x domains on SnO_2 supports resembles that reported previously on ZrO_2 and Al_2O_3 supports [28,35,36].

On MoO_x domains supported on SnO_2, ZrO_2, and Al_2O_3, maximum DME conversion rates (per Mo atom) were obtained at Mo surface densities of 6–7 Mo/nm^2, which resemble those expected for oligomeric two-dimensional struc-

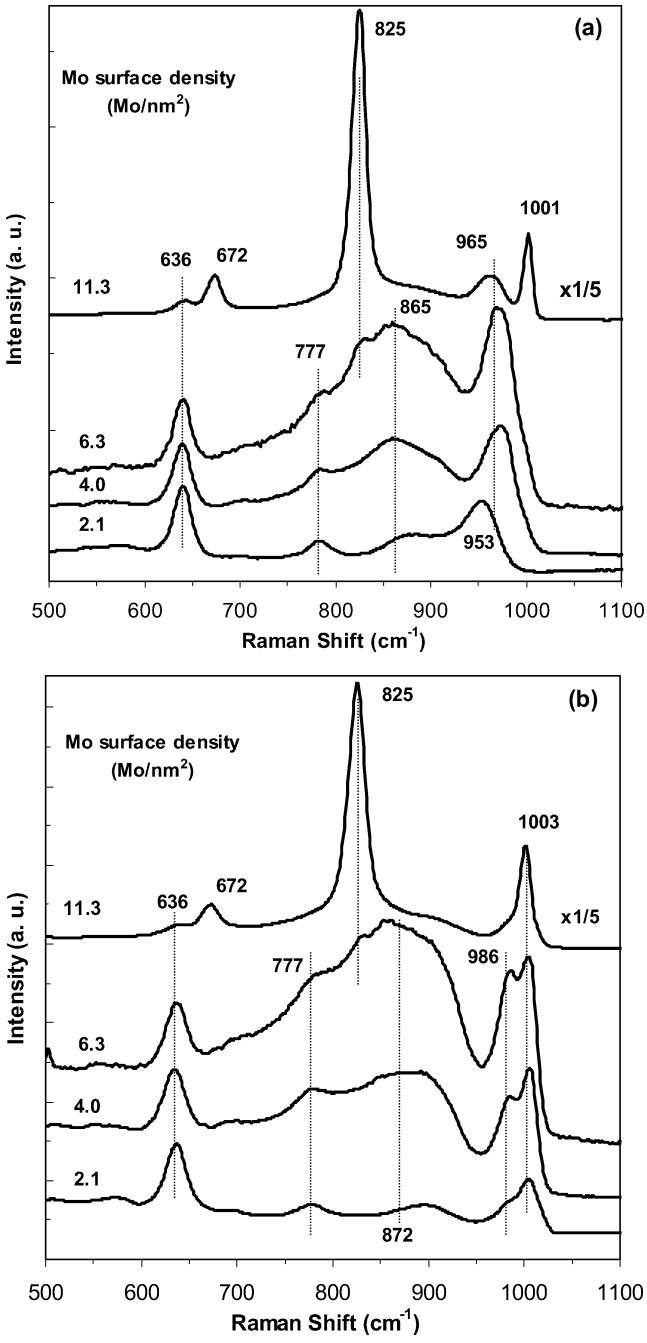

Fig. 1. Raman spectra for MoO_x/SnO_2 catalysts with surface densities of 2.1–11.3 Mo/nm^2 at ambient conditions (a) and after treatment in flowing dry air at 773 K for 1 h (b).

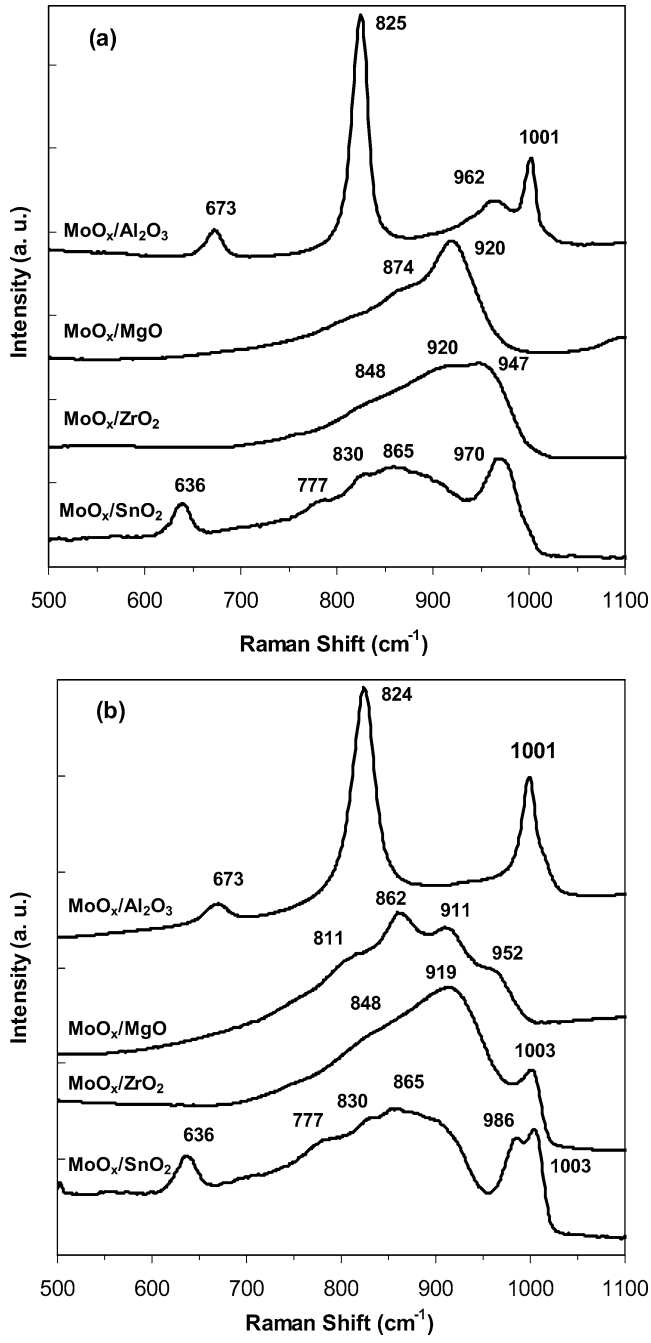

Fig. 2. Raman spectra for supported MoO_x catalysts on MgO, Al_2O_3, ZrO_2, and SnO_2 with surface densities of 5.8–7 Mo/nm^2 at ambient conditions (a) and after treatment in flowing dry air at 773 K for 1 h (b).

tures ($\sim$ 5.0 Mo/nm^2); in contrast, MoO_x/MgO samples showed no detectable catalytic activity (as discussed below).

These support effects on the catalytic properties of MoO_x oligomers were probed first by examining any structural differences detectable in the Raman spectra of samples with different supports but similar surface densities. Figs. 2a and 2b show the Raman spectra for these samples before and after treatment at 773 K in 20% O_2/He, respectively. Before treatment, MoO_x/ZrO_2 (6.4 Mo/nm^2) showed two broad bands at $\sim$ 947 and $\sim$ 850 cm^{-1} and a shoulder at $\sim$ 920 cm^{-1} (Fig. 2a). The removal of water at 773 K shifted the band at $\sim$ 947 to 1003 cm^{-1}, without any detectable changes in the other two bands (Fig. 2b). The bands at $\sim$ 850 and 1003 cm^{-1} arise from Mo–O–Mo and Mo=O vibrational stretches in two-dimensional polymolybdates [24]. The band at $\sim$ 920 cm^{-1} is assigned to symmetric vibrations of O=Mo=O structures in distorted MoO_4 tetrahedral monomers [36] or to Mo–O–Mo stretches in distorted MoO_6 octahedra within two-dimensional oligomers. Raman bands

for MoO_3 were not detected, indicating the absence of three-dimensional crystallites.

The two broad bands at ∼ 874 and 920 cm^{-1} in the fresh MoO_x/MgO sample (5.8 Mo/nm^2) (Fig. 2a) are similar to those reported for aquo MoO_4^{2-} ions, indicating the presence of MoO_4 tetrahedra exposed at MgO surfaces [37]. Water desorption during treatment at 773 K led to Raman bands at 811, 862, 911, and 952 cm^{-1} (Fig. 2b), and to a spectrum similar to that previously reported for MoO_3/MgO (5–7 Mo/nm^2) [37]. The first two bands were assigned to Mo–O–Mo or Mo–O–Mg stretches and the latter two bands to Mo=O symmetric and antisymmetric stretches in polymolybdates [37]. These bands are not associated with crystalline magnesium molybdates, which exhibit sharp bands at ∼ 970, ∼ 950, and 910 cm^{-1} [24,32,37,38]. The structural changes observed on hydration–dehydration are reversible, which precludes the presence of crystalline $MgMoO_4$ structures reported by others [24,38] and suggests instead a reversible tetrahedral-to-octahedral transformation of surface-exposed MoO_x species on water desorption [37].

Fresh MoO_x/Al_2O_3 (7.0 Mo/nm^2) samples showed a broad band at ∼ 962 cm^{-1}, assigned to two-dimensional oligomers [24,28], and three sharper bands at 673, 825 and 1001 cm^{-1}, characteristic of crystalline MoO_3 (Fig. 2a). Treatment at 773 K influenced only the band at ∼ 962 cm^{-1}, which shifted to 1001 cm^{-1} on water desorption. The strong MoO_3 bands in this sample suggest the presence of crystalline MoO_3 structures, but Raman scattering cross sections are 10–10^3 times greater for MoO_3 than for dispersed MoO_x species [39,40]. Thus, we conclude from the similar intensities for the 962 and the 1001 cm^{-1} bands (Fig. 2a) that the sample contains predominately two-dimensional MoO_x oligomers; this conclusion was confirmed by the absence of strong diffraction lines for MoO_3 and by the lack of features in the X-ray absorption fine structure spectra.

The structure of MoO_x domains on these supports (at 6–7 Mo/nm^2) was also probed using radial structure functions obtained from the X-ray absorption fine structure at the Mo *K* edge (Fig. 3). The main feature at ∼ 1.3 Å corresponds to first-shell Mo–O distances, while the much weaker features at ∼ 3.2 Å correspond to Mo–Mo, Mo–Al, Mo–Sn, or Mo–Zr distances. These radial structure functions differ markedly from those measured for crystalline MoO_3 (Fig. 3), which show the largest feature at Mo–Mo distances of ∼ 3.2 Å and two prominent Mo–O bands at ∼ 1.3 and 1.6 Å [41]. Thus, supported MoO_x domains in all samples differ structurally from MoO_3 crystallites, as also concluded from Raman and X-ray diffraction measurements.

3.2. Dimethyl ether reaction rates and HCHO selectivities on supported MoO_x catalysts

Fig. 4a shows primary DME reaction rates per Mo atom at 513 K as a function of Mo surface density on various supports. Rates were always higher on MoO_x/SnO_2 than on MoO_x/ZrO_2 and MoO_x/Al_2O_3. MoO_x/MgO catalysts did not give measurable DME conversions at these reaction conditions. On Al_2O_3, ZrO_2, and SnO_2 supports, rates increased with increasing Mo surface density and reached maximum values at intermediate surface densities of 6–7 Mo/nm^2. For surface densities below those required for maximum rates (per Mo), most Mo atoms in MoO_x domains are accessible to reactants, as discussed in the previous section. Therefore, the reported rates per Mo represent turnover rates and reflect the intrinsic surface reactivity of available MoO_x domains.

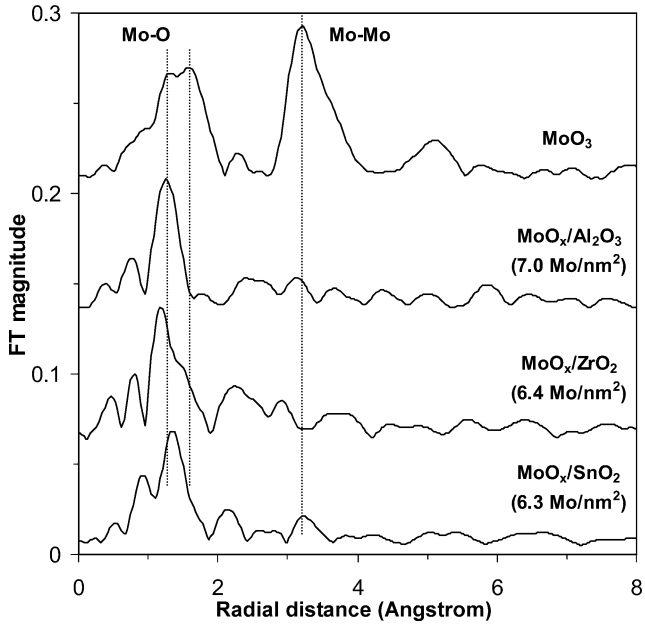

Fig. 3. X-ray absorption radial structure functions for crystalline MoO_3 and for MoO_x domains supported on Al_2O_3, ZrO_2, and SnO_2 after treatment in flowing dry air at 773 K for 1 h.

The observed increase in reaction rates with increasing Mo surface density arises from a higher reactivity of exposed surfaces as the size and dimensionality of MoO_x domains increase. The size of the dispersed MoO_x domains increased monotonically with increasing Mo surface density, as recently shown by changes in the electronic properties of supported MoO_x detected by UV–visible spectroscopy with increasing MoO_x domain size [28,42]. Monomeric species appear to be much less reactive than two-dimensional oligomers and the reactivity of the latter appears to increase with increasing domain size. Larger and more connected MoO_x species are able to delocalize the additional electron density imposed by the reduction part of any catalytic redox cycles, such as those likely to be involved in dimethyl ether oxidation to formaldehyde. As Mo surface densities increased further ($\gtrsim$ 6.5 Mo/nm^2), DME reaction rates (per Mo) decreased, because of the formation of MoO_3 clusters with inaccessible MoO_x structures.

These effects of surface density and domain size are similar to those observed for oxidative dehydrogenation reactions of alkanes on MoO_x and VO_x catalysts [28,42]. As in the case of dehydrogenation reactions, propane oxidation rates increase as electronic transitions between lattice oxy-

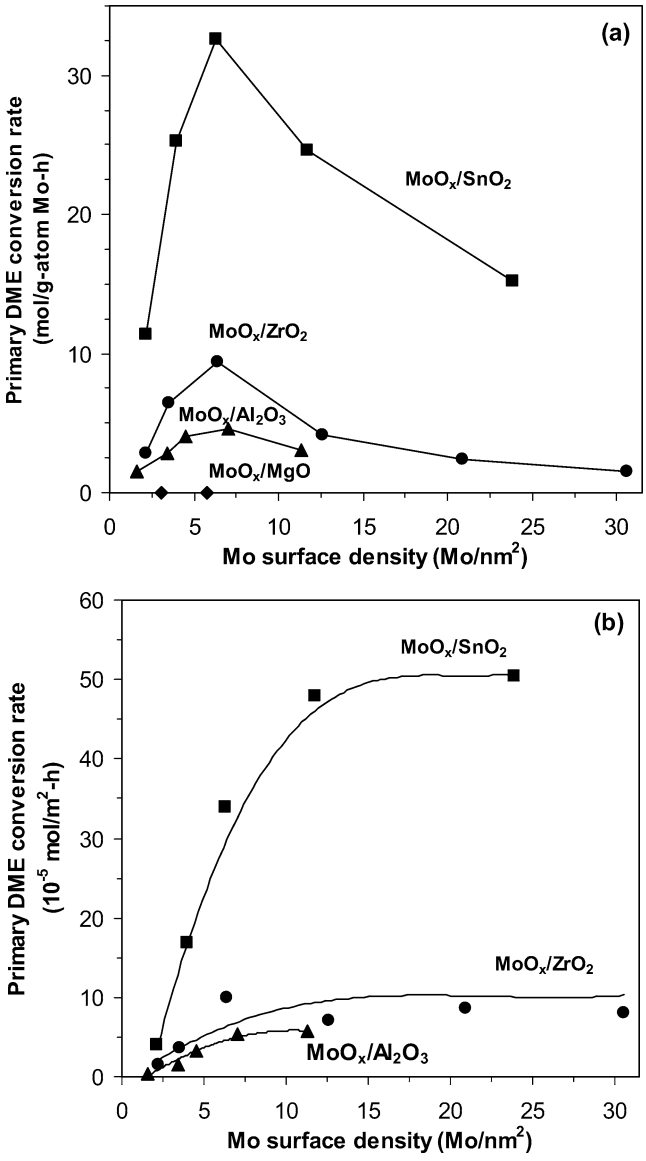

Fig. 4. Primary dimethyl ether conversion rates normalized per Mo atom (a) and normalized per catalyst BET surface area (b) as a function of Mo surface density on MoO_x domains supported on Al_2O_3, ZrO_2, SnO_2, and MgO (513 K; 80 kPa DME, 18 kPa O_2, and 2 kPa N_2).

gen and active metal cations (responsible for the UV–visible absorption edge) decrease in energy [42]. These findings differ markedly from those reported for methanol oxidation reactions on supported VO_x and MoO_x catalysts, for which reaction rates (per active metal atom) appear to be independent of V or Mo content [43,44], even though redox cycles are involved and the oxide domain size strongly influences the reducibility of the active catalytic domains [7,28].

Areal DME reaction rates were estimated for each supported MoO_x sample based on their total BET surface areas. Areal rates increased with increasing Mo surface density (Fig. 4b) and reached nearly constant values for surface densities above 6–7 Mo/nm^2 on all supports. These trends suggest that support surfaces become entirely covered with MoO_x structures and that any MoO_x species in excess of the amount required to form an active polymolybdate monolayer lead to MoO_x crystallites, which do not contribute appreciably to the exposed active surface area or to the measured reaction rates. These asymptotic areal rates, however, depend on the identity of the support, as expected from the existing atomic connectivity between MoO_x layers and oxygen atoms on support surfaces (Table 1). Constant areal rates of about 6, 9, and 50×10^{-5} mol/(m^2 h) were obtained on MoO_x/Al_2O_3, MoO_x/ZrO_2, and MoO_x/SnO_2, respectively, as each sample approached polymolybdate monolayer coverages. At low surface densities, the exposed inactive regions on support surfaces lead to low calculated areal rates, which increase as these regions become covered with monomeric molybdates of low intrinsic activity and ultimately with more active MoO_x oligomers.

Oxidative DME reactions on MoO_x-based catalysts proceed via primary and secondary pathways depicted in Scheme 1 [20]. These pathways include the direct conversion of DME to CH_3OH (k_0), HCHO (k_1), methyl formate (MF) (k_2), and CO_x ($CO + CO_2$) (k_3) in one surface sojourn. They also include secondary reactions of HCHO to form MF (k_4) and CO_x (k_5) and of MF to form CO_x (k_6). In each case, k_i represents the rate constant for reaction i. At the low conversions of this study, all primary reactions can be assumed to be pseudo-zero order in DME and O_2, because their respective concentrations remain nearly constant with changes in reactant residence time or conversion [20]. Secondary reactions are assumed to be pseudo-first order in the concentration of the primary product involved, but any kinetic dependencies on DME and O_2 are neglected for the same reasons proposed for primary reactions. Traces of dimethoxymethane (DMM) were also detected, but are not included in the reaction scheme because of the low selectivities ($< 1\%$). CH_3OH selectivities were largely unaffected by residence time, suggesting that CH_3OH is formed directly as a co-product of HCHO formation. Its alternate formation via DME hydration would require H_2O co-reactants, which are

Table 1
Some results on MoO_x supported on Al_2O_3, ZrO_2, and SnO_2 with surface densities of 11.3–12.6 Mo/nm^2 as well as on MgO (5.8 Mo/nm^2)

Support	Areal rate (10^{-5} mol/(m^2 h))	Primary HCHO selectivity (%)	$k_1/(k_2+k_3)$	$k_1/((k_4+k_5)C_{A_0})$
Al_2O_3	5.7	98.0	47.0	0.35
ZrO_2	7.5	81.8	4.5	0.08
SnO_2	48.0	88.4	7.6	0.10
MgO	0.0	–	–	–

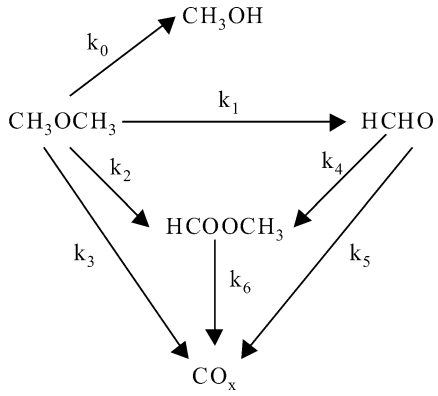

Scheme 1. Primary and secondary reaction pathways for dimethyl ether conversion on MoO_x-based catalysts

not available at low conversions. The weak effects of residence time on CH_3OH indicate also that CH_3OH oxidation is slower than DME oxidation under these reaction conditions.

The rate constants k_1, k_2, and k_3 were calculated from the corresponding pseudo-zero-order primary reaction rates, and $(k_4+k_5)C_{A_0}$ (C_{A_0} = inlet DME concentration) from the observed changes in HCHO selectivity (S_B) with ν as given by

$$S_B = S_B^0\left[1 - \tfrac{1}{2}(k_4+k_5)C_{A_0}\cdot\nu\right],$$

where S_B^0 is the primary HCHO selectivity, C_{A_0} is the inlet DME concentration, and ν = g-atom Mo/inlet molar DME rate (g-atom Mo-s/mol DME). S_B^0 is given by $k_1/(k_1+k_2+k_3)$ (on a CH_3OH-free basis) [20].

Primary HCHO selectivities on MoO_x/ZrO_2 and MoO_x/SnO_2 catalysts increased monotonically with increasing Mo surface density and reached constant values of ∼ 90% for surface densities higher than 6–7 Mo/nm^2 (Fig. 5a). Concurrently, primary MF and CO_x ($CO+CO_2$) selectivities decreased to constant values of ∼ 7 and 3% (Figs. 5b and 5c). This indicates that exposed SnO_2 and ZrO_2 surfaces or Mo–O–Sn(Zr) structures show higher MF and CO_x selectivities than Mo–O–Mo structures, as also reported for CH_3OH oxidation reactions [43,45,46]. Yet, none of these supports led to significant DME conversion rates in the absence of MoO_x active species. On MoO_x/Al_2O_3, MF (2–4%) and CO_x (0–1.2%) selectivities were very low and nearly independent of Mo surface density (Figs. 5b and 5c), while HCHO selectivities increased only slightly from 95.2 to 98.1% as the Mo surface density increased from 1.6 to 11.3 Mo/nm^2 (Fig. 5a). Thus, it appears that Mo–O–Al structures are essentially unreactive in DME conversion reactions to MF and CO_x. These results show that the coverage of the support surfaces with active MoO_x domains favor high HCHO selectivities, especially in the case of more reducible ZrO_2 and SnO_2 supports.

The redox properties of MoO_x domains influence DME oxidation rates (as discussed below), while acid–base properties may influence reactions of DME-derived adsorbed in-

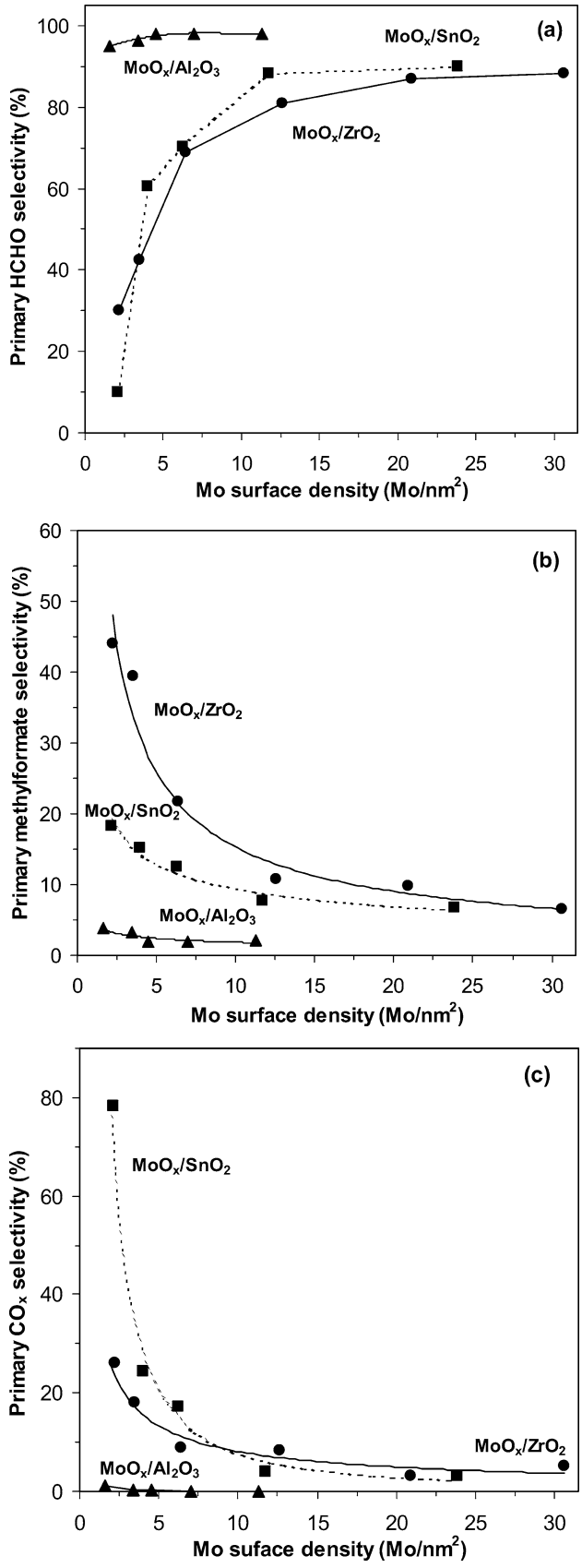

Fig. 5. Primary selectivities to HCHO (a), methyl formate (b), and CO_x (c) as a function of Mo surface density on supported MoO_x catalysts on Al_2O_3, ZrO_2, and SnO_2 (513 K; 80 kPa DME, 18 kPa O_2, and 2 kPa N_2).

termediates, as well as the readsorption and secondary reactions of HCHO. DME oxidation proceeds via methoxy groups formed by DME dissociation on Mo–O sites, followed by a reduction step involving C–H bond activation in methoxy groups ($CH_3O^{\delta-}$) using lattice oxygen [47]. High primary HCHO selectivities require that adsorbed HCHO species desorb before subsequent reactions. More acidic and less reducible surfaces favor HCHO desorption, while inhibiting the formation of strongly adsorbed dioxymethylene and formate species, which require nucleophilic attack by basic lattice oxygens to form ultimately MF and CO_x. It appears that exposed ZrO_2 and SnO_2 surfaces or heteroatomic Mo–O–support linkages prevalent at surface densities below 6–7 Mo/nm^2 provide strong binding sites for $CH_3O^{\delta-}$ and HCHO. Similar effects have been proposed for methanol oxidation reactions [45,46]. Infrared and desorption studies of adsorbed methanol detected the presence of strongly adsorbed dioxymethylene and formate species on SnO_2 and ZrO_2 surfaces, which led only to CO_x, while more weakly adsorbed $CH_3O^{\delta-}$ species on MoO_x species formed HCHO [45,46].

Figs. 6a and 6b show $k_1/(k_2+k_3)$ and $k_1/((k_4+k_5)C_{A_0})$ values, respectively, as a function of Mo surface density for all samples. Values of $k_1/(k_2+k_3)$ reflect primary DME conversion rates to HCHO (k_1) relative to those for MF (k_2) and CO_x (k_3) formation; thus, they provide an alternate measure of primary HCHO selectivities. In contrast, $k_1/((k_4+k_5)C_{A_0})$ ratios (at a constant inlet DME concentration, C_{A_0}) reflect primary HCHO formation rates (k_1) relative to the rates for secondary HCHO reactions to form MF (k_4) and CO_x (k_5); this kinetic parameter reflects the tendency of a given catalyst to form and convert HCHO. High values of $k_1/(k_2+k_3)$ and $k_1/((k_4+k_5)C_{A_0})$ lead to higher HCHO selectivities for a given DME conversion; the second parameter becomes increasingly important in determining HCHO yields as DME conversion increases.

Both $k_1/(k_2+k_3)$ and $k_1/((k_4+k_5)C_{A_0})$ ratios increased with increasing Mo surface density and reached constant values above 6–7 Mo/nm^2 on MoO_x/Al_2O_3, MoO_x/ZrO_2, and MoO_x/SnO_2 (Fig. 6). Thus, the increasing coverage of the support with MoO_x species and the larger MoO_x domains formed as surface density increases led to more selective catalytic surfaces and to higher HCHO yields. The higher $k_1/(k_2+k_3)$ and $k_1/((k_4+k_5)C_{A_0})$ values on MoO_x domains supported on Al_2O_3 relative to those on SnO_2 and ZrO_2 at the constant C_{A_0} suggest that more reducible supports with weak Lewis acidity favor the conversion of adsorbed HCHO species to MF and CO_x, as discussed above. Apparently, such supports allow Mo cations in MoO_x domains to become more electron-rich, thus lowering their affinity for binding electron-donating DME-derived intermediates and HCHO. Similar effects of the Lewis acidity of active oxide cations and of the supports have been reported for secondary reactions of alkenes during oxidative dehydrogenation of alkanes on VO_x, MoO_x, and WO_x catalysts [48]. In this case, electron-rich alkenes interact

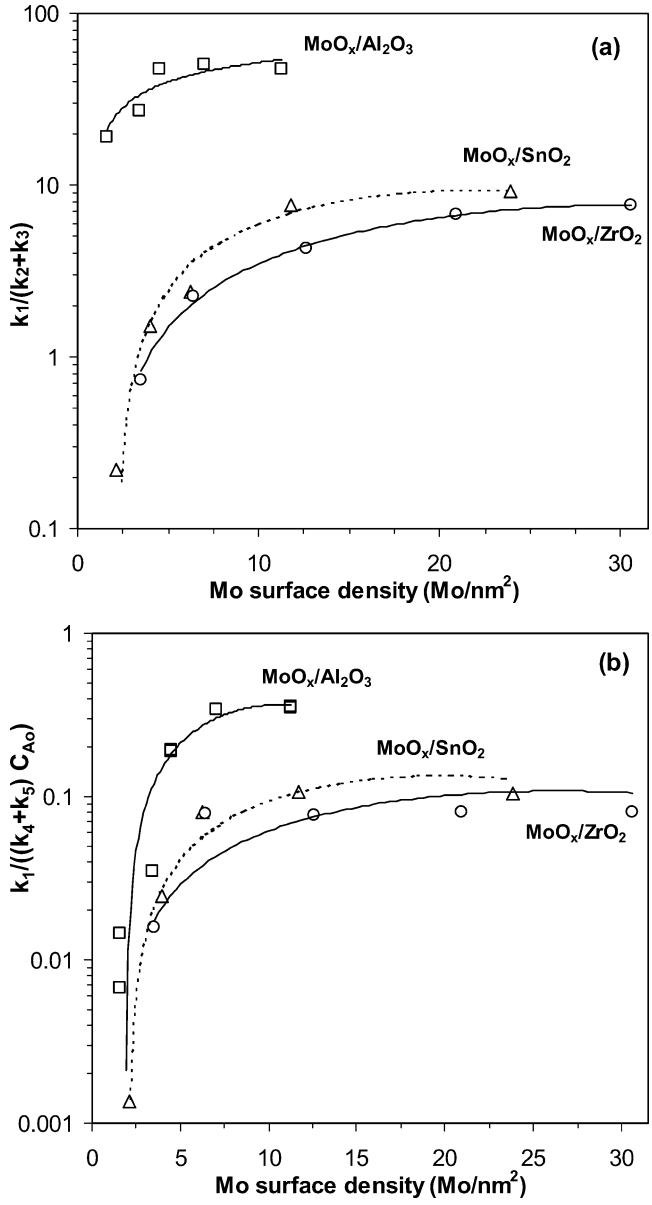

Fig. 6. Rate constant ratios $k_1/(k_2+k_3)$ (a) and $k_1/((k_4+k_5)C_{A_0})$ (C_{A_0}; inlet DME concentration) (b) (presented in a logarithmic scale) as a function of Mo surface density on MoO_x domains supported on Al_2O_3, ZrO_2, and SnO_2 (513 K; 80 kPa DME, 18 kPa O_2, and 2 kPa N_2).

strongly with more acidic active metal cations, leading to longer surface residence times during their initial formation from alkanes and to a greater tendency for them to readsorb and undergo secondary combustion reactions.

Next, we turn our attention to the underlying basis for the observed support effects on DME reaction rates and HCHO selectivity. DME reaction rates are significantly higher for MoO_x domains supported on SnO_2 than for those on ZrO_2 or Al_2O_3, even when polymolybdate monolayers are prevalent on all supports; in contrast, MoO_x species on MgO are inactive (Fig. 4, Table 1). Unreducible Al_2O_3 supports give higher HCHO selectivities than ZrO_2 or SnO_2 (Fig. 5). The $k_1/(k_2+k_3)$ and $k_1/((k_4+k_5)C_{A_0})$

values decreased from 47 and 0.35 on Al_2O_3 to 8–9 and 0.08–0.10 on ZrO_2 and SnO_2 at the constant C_{A_0}, respectively (Fig. 6). Clearly, the chemical properties of a polymolybdate monolayer depend on the identity of the underlying support to which it is atomically connected. In the next section, we examine the effects of support on MoO_x reduction properties for catalysts containing predominately polymolybdate monolayers (6–7 Mo/nm^2).

3.3. Genesis of support effects in dimethyl ether oxidation on MoO_x domains

For Mo surface densities of 6–7 Mo/nm^2, all MoO_x species on Al_2O_3, ZrO_2, SnO_2, and MgO supports are accessible to reactants; therefore, differences in accessibility cannot account for the observed effects of supports on DME reaction rates. Kinetic and isotopic studies have shown that HCHO formation from DME involves redox cycles and kinetically relevant C–H bond activation steps [47]. The transition states required for such C–H bond activation steps involve the incipient local reduction of MoO_x domains to form an OH group and adsorbed HCHO species bound to a metal cation. Reactions limited by C–H bond activation on metal oxides, such as oxidative alkane dehydrogenation on MoO_x and VO_x, show excellent correlations between catalytic reaction rates and the electronic and redox properties of oxide domains [42]. Thus, we suggest that the strong support effects observed for DME oxidation reactions also reflect differences in the reducibility of MoO_x domains on the various supports.

The rates of reduction of supported MoO_x domains were measured using H_2 as the stoichiometric reductant while the sample temperature was increased from 298 to 1253 K. Specifically, the rates of the incipient reduction of Mo^{6+} to Mo^{4+} were measured. In-situ X-ray absorption spectra showed that few reduced Mo centers are present during steady-state DME reactions at 513 K [47]. Thus, the initial stages of Mo^{6+} reduction are the chemical processes most relevant to the redox cycles required for catalytic turnovers, as discussed in detail elsewhere for related oxidation reactions [28,42].

Fig. 7 shows incipient reduction rates in H_2 (at 623 K) as a function of Mo surface density for MoO_x domains supported on ZrO_2, Al_2O_3, and MgO at surface densities of 6–7 Mo/nm^2, as well as for three other ZrO_2-supported samples with Mo surface densities of 0.5, 3.5, and 5.6 Mo/nm^2 and for a MoO_x/Al_2O_3 sample with 3.4 Mo/nm^2. These incipient H_2 reduction rates increased with increasing Mo surface density for each support. They were higher on MoO_x/ZrO_2 than on MoO_x/Al_2O_3 and MoO_x/MgO catalysts for a given surface density. For MoO_x/SnO_2, however, the extensive concurrent reduction of MoO_x domains and of the SnO_2 support precludes the use of this method to measure MoO_x reduction rates.

Fig. 8 shows a parallel increase in the rate of primary DME conversion (513 K) and in the rate of incipient

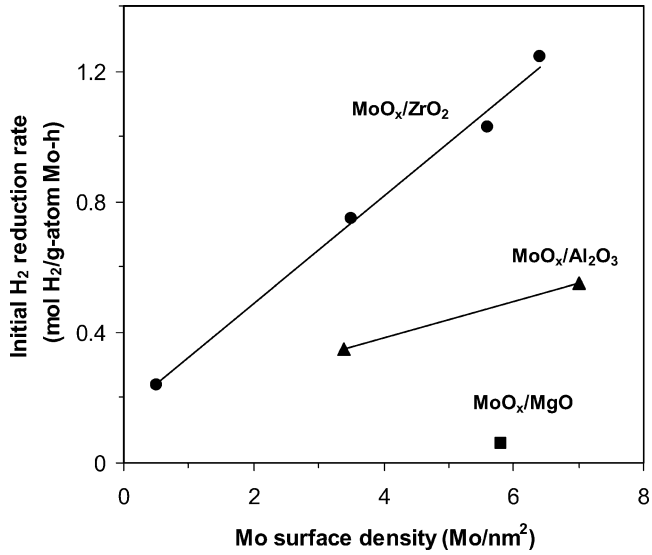

Fig. 7. Incipient reduction rates in H_2 (at 623 K) for MoO_x domains supported on ZrO_2 (●), Al_2O_3 (▲), and MgO (■) at similar Mo surface densities (5.8–7 Mo/nm^2), on MoO_x/Al_2O_3 (3.4 Mo/nm^2) (▲), and on MoO_x/ZrO_2 with 0.5, 3.5, and 5.6 Mo/nm^2 (●).

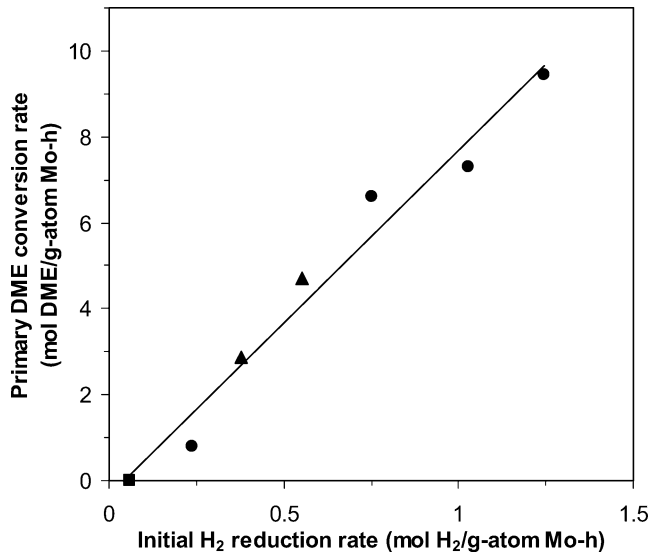

Fig. 8. Relationship between primary DME reaction rates (513 K) and initial H_2 reduction rates (623 K) for MoO_x domains supported on ZrO_2 (●), Al_2O_3 (▲), and MgO (■) at similar Mo surface densities (5.8–7 Mo/nm^2), on MoO_x/Al_2O_3 (3.4 Mo/nm^2) (▲), and on MoO_x/ZrO_2 with 0.5, 3.5, and 5.6 Mo/nm^2 (●).

stoichiometric reduction in H_2 (623 K) for the samples shown in Fig. 7. On these samples, MoO_x species are predominately exposed at surfaces and accessible to both DME and H_2 reactants. Thus, the measured reaction rates (per Mo) reflect the reactivity of exposed surfaces for the two respective reactions. Clearly, the tendency of these domains to undergo reduction with the generation of a small number of oxygen vacancies increases in parallel with their ability to catalyze DME reaction turnovers, which appear to involve

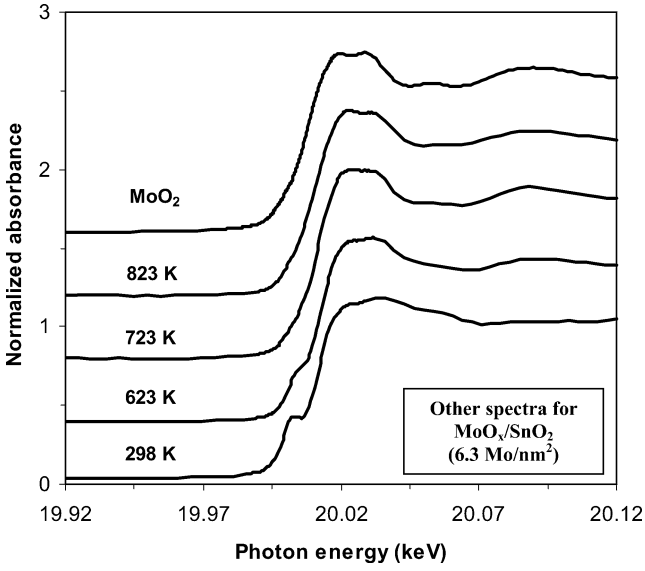

Fig. 9. X-ray absorption spectra near the Mo K edge for MoO_x/SnO_2 (6.3 Mo/nm^2) after treatment in H_2 (20% H_2/Ar) at 298, 623, 723, and 823 K and for crystalline MoO_2 at ambient temperature.

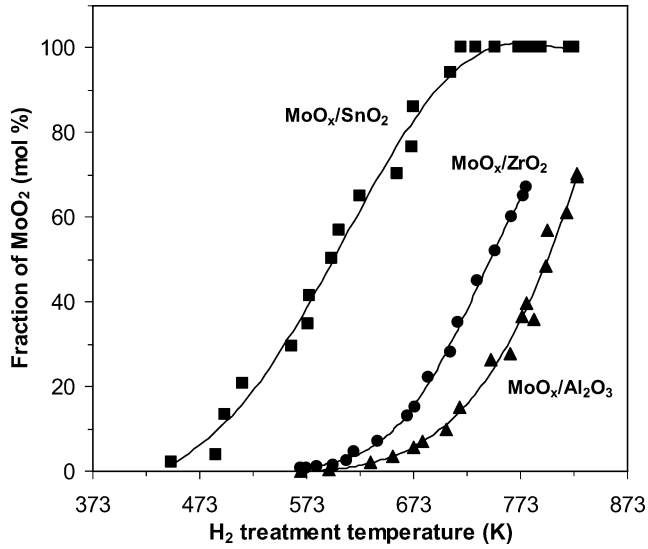

Fig. 10. MoO_2 fraction measured from linear superimposition of MoO_2 and initial spectra as a function of treatment temperature in 20% H_2/Ar for MoO_x domains supported on Al_2O_3, ZrO_2, and SnO_2 at similar Mo surface density (6.3–7 Mo/nm^2).

the Mars–van Krevelen pathways [49] involving reducible centers and lattice oxygen atoms.

The difficulties caused by the concurrent reduction of MoO_x and SnO_2 led us to examine the dynamics of reduction in H_2 at 298–823 K using in situ X-ray absorption features near the Mo K edge for MoO_x domains on SnO_2, ZrO_2, and Al_2O_3 with similar surface densities (6–7 Mo/nm^2). The concentrations of Mo^{6+} and Mo^{4+} were estimated by linear superimposition methods using the starting spectrum and the spectrum of MoO_2 as principal components. The Mo K absorption edge arises from the ejection of a 1s photoelectron, while the pre-edge feature at $\sim$ 19.99 keV corresponds to a 1s-to-4d transition that is dipole-forbidden in centrosymmetric structures [29,41]. The Mo^{6+} cations in MoO_3 adopt off-center positions within distorted MoO_6 octahedra, which lead to p–d orbital hybridization and to a detectable pre-edge feature in the MoO_3 spectrum. In contrast, MoO_2 has only a very weak pre-edge feature. Recently, Ressler et al. [41] and Chen et al. [28] reported reduction rates for crystalline MoO_3 and supported MoO_3/Al_2O_3, respectively, from linear superimposition of Mo K edge spectra.

Fig. 9 shows the Mo K near-edge spectra for MoO_x/SnO_2 (6.3 Mo/nm^2) during contact with 20% H_2/Ar at 298, 623, 723, and 823 K, and for crystalline MoO_2 at ambient conditions. The pre-edge feature weakened with increasing temperature and the spectral features approached those typical of MoO_2. Above 723 K, all spectra are accurately described using only the MoO_2 standard spectrum, without any spectral contributions from either the starting sample or crystalline MoO_3. Below 723 K, the spectra are accurately described by linear combinations of the spectra for the initial sample and for crystalline MoO_2.

Fig. 10 shows the fraction of the Mo cations present as Mo^{4+} as a function of temperature for the three supported samples with surface densities of 6–7 Mo/nm^2. The Mo^{4+} fraction is significantly greater for MoO_x/SnO_2 than for MoO_x/ZrO_2 and MoO_x/Al_2O_3 at all temperatures, indicating that MoO_x species dispersed on SnO_2 are easier to reduce than on the other two supports. A similar trend was observed for the reactivity of MoO_x species in these samples for DME reactions (Fig. 4). MoO_x domains supported on SnO_2 appear to delocalize the electron density that they acquire during stoichiometric reduction processes and also during reduction steps involved in C–H bond activation steps within each catalytic redox cycle. Clearly, the reducibility of the support itself must play a role in these effects, because a shift from refractory MgO and Al_2O_3 supports to more reducible ZrO_2 and SnO_2 leads to concomitant changes in the reduction properties of the supported MoO_x domains.

The observed parallel increases in the reducibility and catalytic reactivity of the active oxides is similar to those observed for other reactions catalyzed by supported MoO_x and VO_x, such as the oxidative dehydrogenation of alkanes [28, 31,50] and alcohols [43,44]. These findings are consistent with the involvement of lattice oxygen atoms and of transition states with significant reduction of metal centers in the catalytic cycles required for DME conversion to HCHO [47]. These relationships and mechanistic inferences provide the basis for the catalytic improvements that we have achieved by surface modifications of Al_2O_3 supports, in an effort to increase the reactivity of supported MoO_x domains, without loss of the selective properties of Al_2O_3-supported MoO_x domains for DME conversion to HCHO [51].

4. Conclusions

MoO_x domains on Al_2O_3, ZrO_2, and SnO_2 catalyze the selective oxidation of dimethyl ether to HCHO at 453–553 K. No reaction products, however, were detected on MoO_x domains supported on MgO at similar surface densities. On all supports, the size and dimensionality of MoO_x domains increased with increasing MoO_x surface density. MoO_3 clusters were first detected by Raman spectroscopy at surface densities of 6–7 Mo/nm^2, which correspond to those expected for two-dimensional MoO_x monolayers. Primary HCHO synthesis rates (per Mo atom) were influenced by the Mo surface density on each support. These rates initially increased with increasing MoO_x surface density on all supports up to 6–7 Mo/nm^2, indicating that the surface reactivity of MoO_x domains increases as a two-dimensional monolayer forms via oligomerization of monomolybdate species. Ultimately, the incipient formation of three-dimensional MoO_3 clusters leads to some inaccessible MoO_x species and lower reaction rates (per Mo). Areal reaction rates reached a constant value as the polymolybdate monolayers form, but these areal rates were highest on SnO_2 supports and lowest on Al_2O_3, indicating that the catalytic properties of these polymolybdate layers depend strongly on the chemical identity of the support surfaces to which they are atomically attached. These domain size effects appear to reflect the effectiveness of larger domains to delocalize charge, which is required for kinetically relevant steps in the redox cycles involved in HCHO synthesis. This proposal is consistent with the faster rates of incipient reduction using H_2 with increasing MoO_x surface density and with changes in support. The domain size and the identity of the support influence charge delocalization properties of MoO_x domains and thus their catalytic and reduction rates. Reaction rates (per Mo atom) for supported samples with 6–7 Mo/nm^2 are significantly higher on SnO_2 than on ZrO_2 or Al_2O_3 supports. Similar trends were observed for stoichiometric reduction rates of these samples using H_2. The effects of support on primary and secondary HCHO selectivities is consistent with the weaker binding of DME-derived intermediates and of HCHO on Mo^{6+} sites with higher Lewis acidity; these sites favor desorption of HCHO precursors, while discouraging HCHO readsorption and secondary reactions to form CO_x and methyl formate.

Acknowledgments

This study was supported by BP as part of the Methane Conversion Cooperative Research Program at the University of California at Berkeley. The authors thank Dr. Kaidong Chen for synthesis of some of the Al_2O_3-supported MoO_x samples. The authors also acknowledge helpful technical discussions with Dr. Theo Fleisch and Dr. John Collins of BP.

References

[1] R. Pitchai, K. Klier, Catal. Rev. Sci. Eng. 28 (1986) 13.
[2] J.S. Lee, S.T. Oyama, Catal. Rev. Sci. Eng. 30 (1988) 249.
[3] K. Tabata, Y. Teng, T. Takemoto, E. Suzuki, M.A. Banares, M.A. Pena, J.L. Garcia Fierro, Catal. Rev. Sci. Eng. 44 (2002) 1.
[4] K. Otsuka, Y. Wang, Appl. Catal. 222 (2001) 145.
[5] I.C. Bafas, I.E. Constantinou, C.G. Vayenas, Chem. Eng. J. 82 (2001) 109.
[6] L. Lefferts, J.G. van Ommen, J.R.H. Ross, Appl. Catal. 23 (1986) 385.
[7] J.M. Tatibouet, Appl. Catal. A 148 (1997) 213.
[8] J.-L. Li, X.-G. Zhang, T. Inui, Appl. Catal. A 147 (1996) 23.
[9] T.H. Fleisch, A. Basu, M.J. Gradassi, J.G. Masin, Stud. Surf. Sci. Catal. 107 (1997) 117.
[10] T. Shikada, Y. Ohno, T. Ogawa, M. Ono, M. Mizuguchi, K. Tomura, K. Fujimoto, Stud. Surf. Sci. Catal. 119 (1998) 515.
[11] M. Hara, M. Kawamura, J.N. Kondo, K. Domen, K. Maruya, J. Phys. Chem. 100 (1996) 14462.
[12] F. Ouyang, S. Yao, J. Phys. Chem. 104 (2000) 11253.
[13] H. Tadenuma, T. Murakami, H. Mitsushima, US Patent 3,655,771.
[14] R.M. Lewis, R.C. Ryan, L.H. Slaugh, US Patent 4,442,307, 1984.
[15] R.M. Lewis, R.C. Ryan, L.H. Slaugh, US Patent 4,439,624, 1984.
[16] R.M. Lewis, R.C. Ryan, L.H. Slaugh, US Patent 4,435,602, 1984.
[17] G.P. Hagen, M.J. Spangler, US Patent 6,265,528, 2001.
[18] G.P. Hagen, M.J. Spangler, US Patent 6,350,919, 2002, assigned to BP.
[19] H. Liu, E. Iglesia, J. Catal. 208 (2002) 1.
[20] H. Liu, P. Cheung, E. Iglesia, J. Phys. Chem., in press.
[21] A.N. Desikan, L. Huang, S.T. Oyama, J. Chem. Soc. Faraday Trans. 88 (1993) 3357.
[22] A. Auroux, D. Sprinceana, A. Gervasini, J. Catal. 195 (2000) 140.
[23] D.S. Kim, K. Segawa, T. Soeya, I.E. Wachs, J. Catal. 136 (1992) 539.
[24] G. Mestl, T.K.K. Srinivasan, Catal. Rev. Sci. Eng. 38 (1998) 451.
[25] M. Niwa, Y. Matsuoka, Y. Murakami, J. Phys. Chem. 91 (1987) 4519.
[26] X. Gao, E. Wachs, Top. Catal. 18 (2002) 243.
[27] A. Khodakov, B. Olthof, A.T. Bell, E. Iglesia, J. Catal. 181 (1999) 205.
[28] K. Chen, S. Xie, A.T. Bell, E. Iglesia, J. Catal. 198 (2001) 232.
[29] W. Li, G.D. Meitzner, R.W. Borry III, E. Iglesia, J. Catal. 191 (2000) 373.
[30] T. Ressler, WinXAS 97, Version 1.2, 1998.
[31] K. Chen, S. Xie, A.T. Bell, E. Iglesia, J. Catal. 195 (2000) 244.
[32] S.R. Stampel, Y. Chen, J.A. Dumesic, C. Niu, C.G. Hill Jr., J. Catal. 105 (1987) 445.
[33] B. Amram, H. Pernot, A.M. Govic, M. Gubelmann-Bonneau, Vibr. Spectrosc. 9 (1995) 65.
[34] Y.C. Xie, Y.Q. Tang, Adv. Catal. 37 (1990) 1.
[35] K. Chen, S. Xie, E. Iglesia, A.T. Bell, J. Catal. 189 (2000) 421.
[36] S. Xie, K. Chen, A.T. Bell, E. Iglesia, J. Phys. Chem. 104 (2000) 10059.
[37] S.-C. Chang, M.A. Leugers, S.R. Bare, J. Phys. Chem. 96 (1992) 10358.
[38] D.S. Kim, I.E. Wachs, K. Segawa, J. Catal. 146 (1994) 268.
[39] R. Radhakrishnan, C. Reed, S.T. Oyama, M. Semen, J.N. Kondo, K. Domen, Y. Ohminami, K. Asakura, J. Phys. Chem. 105 (2001) 8519.
[40] C.C. Williams, J.G. Ekerdt, J.M. Jehng, F.D. Hardcastle, I.E. Wachs, J. Phys. Chem. 95 (1991) 9791.
[41] T. Ressler, O. Timpe, T. Neisius, J. Find, G. Mestl, M. Dieterle, R. Schlogl, J. Catal. 191 (2000) 75.
[42] K. Chen, A.T. Bell, E. Iglesia, J. Catal. 209 (2002) 35.
[43] G. Deo, I.E. Wachs, J. Catal. 146 (1994) 323.
[44] W. Zhang, A. Desikan, S.T. Oyama, J. Phys. Chem. 99 (1995) 14468.
[45] M. Niwa, J. Igarashi, Catal. Today 52 (1999) 71.
[46] N. Narishige, M. Niwa, Catal. Lett. 71 (2001) 63.
[47] H. Liu, P. Cheung, E. Iglesia, unpublished results.
[48] K. Chen, A.T. Bell, E. Iglesia, J. Phys. Chem. 104 (2000) 1292.
[49] P. Mars, D.W. van Krevelen, Chem. Eng. Sci. 3 (1954) 41.
[50] M.C. Abello, M.F. Gomez, L.E. Cadus, Catal. Lett. 83 (1998) 185.
[51] H. Liu, P. Cheung, E. Iglesia, Phys. Chem.